SPHysics Code Validation Against a Near–Shore Wave Breaking Experiment

Christos V. Makris, Yannis N. Krestenitis
Dept. of Civil Engineering
Aristotle University of Thessaloniki (AUTh)
Thessaloniki, Greece
cmakris@civil.auth.gr, ynkrest@civil.auth.gr

Constantine D. Memos
School of Civil Engineering
National Technical University of Athens (NTUA)
Athens, Greece
memos@hydro.ntua.gr

***Abstract*—The use of the academic 'open source' code SPHysics, in the framework of wave breaking simulation over a relatively mild–sloping beach, is discussed in this paper. Thorough calibration of the relevant code's wide range of parameters and assumptions is attempted through the comparison between numerical and experimental data. A general validation of the Smoothed Particle Hydrodynamics (SPH) method's ability to capture the dynamics of near–shore wave breaking features and the characteristics of surf and swash zone turbulence, is implemented. Plausible qualitative agreement is achieved and inherent drawbacks and calibration weaknesses of the model are detected, based upon quantitative discrepancies. Moreover, particular amendments of the classic Smagorinsky–type turbulence model, incorporated in SPHysics, are suggested and the use of a more efficient one is introduced, setting the grounds for prospective research.**

I. INTRODUCTION

Coastal engineers and scientists are deeply concerned about the comprehension and the description of the detailed near–shore wave pattern evolution, in their effort to examine the extremely complex character of coastal processes. Among those, wave propagation, shoaling and depth–induced breaking are dominant. Specifically the latter is of major significance in assessing the surf/swash zone characteristics, such as the breaker wave height and type, the velocity and vorticity profiles, the undertow return–type flow, the shoreward net drift–type motion (Stokes's drift), the overall coherent and intermittent turbulent structures etc. All the above primarily control coastal sediment movements, thus long– and cross–shore morphodynamic evolution and secondarily the aeration and mixing processes inside the surf zone. The latter combined with the descending turbulent eddy formation, are responsible for the definition of quality and safety criteria for recreation and related activities. Moreover, climate change may aggravate consequent hazardous inundation events by extreme waves surging on especially low–land beach formations. Relative run–up on mild–sloping coasts as well as scouring due to turbulence at the toe of the associated steeper coastal protection works are of great importance.

Accordingly, near–shore wave breaking and related turbulence have been investigated adequately both physically and numerically, throughout the last decades, mostly accounting for the surf zone and secondarily for the swash and run–up ones. Despite that, the hydrodynamics describing the respective processes are far from completely elucidated. In this framework, laboratory experiments have been conducted, implementing various measuring techniques and introducing physical modelling of wave generation, propagation and breaking of the spilling or plunging type, on inclined beach slopes placed inside small scale wave flumes. Such are the photographic depiction of the breaking wave with simultaneous measurements of the free surface at specific gauge points throughout the propagation, surf and swash zone regions and the more elaborate modern Acoustic/Laser Doppler Velocimetry (ADV/LDV) or Anemometry (LDA), e.g. those used by [1] to trace obliquely descending eddies and more recent researches presented below. Furthermore Particle Image Velocimetry (PIV) methods [2] are frequently used nowadays, covering broader areas than gauges by recording high frequency frames of the flow field, thus depicting its overall turbulent patterns and structures. Extended and thorough reviews on the matter can be found in [3] and [4], while [5] focuses on the swash zone dynamics. On the other hand modern computational approaches comprise modelling of the full Navier–Stokes (NS) equations in combination with averaging and surface tracking techniques like RANS–VOF or Large Eddy Simulation (LES) models combined with Sub–Grid Scale (SGS) turbulence closure ones. Smoothed Particle Hydrodynamics (SPH) [6], [7] is the most widely discerned mesh–free (particle) method, used in several fields, especially standing out as a pledging modern technique in dealing with highly deformed free surface flows (e.g. plunging breakers), incorporating Lagrangian numerical formulation and rendering dispensable the strenuous employment of a toggling computational grid [8]. The implementation of SPH to a broad range of problems has guided researchers to important numerical corrections of the original SPH method, like moving the particles with the XSPH variant [9], re–initialising the density of the particles [10], incorporating Moving Least Squares (MLS) approach [11], introducing kernel [12] and kernel gradient corrections and dealing with tensile instabilities [13]. All of the above are taken into account in the present study through use of the recently issued academic 'open source' code SPHysics [14]. Some of the very recent proficient

improvements, like the use of Riemann solvers [15], accurate and stable incompressible SPH [16] and consistent wall modelling for solid boundary conditions [17], are not incorporated in our research.

The prompt goal of the present study is the exact simulation of the highly nonlinear process of wave breaking on plane and relatively mild impermeable slopes. In the long run, we aim at quantifying the undertow and run–up on sloping beaches. Moreover, a detailed description of the turbulent features inside the surf and swash zones is pursued and all of the above, by means of validating the SPHysics results against those of one of the most recent comprehensive laboratory experimental studies on near–shore breaking waves and consequent turbulence transport under them [18]. Calibration of the various parameters of the SPHysics code is being attempted and the key features are evinced through inter–comparisons of several implementations. Extensive comparative analysis between the model and the experiment results is presented here, shedding some light to the limitations of the model application and indicating specific upgrades for future research. The important role of the smoothing kernel function and length *h*, in terms of computational accuracy, is proved. Moreover, the artificial viscosity assumption [6] is applied, yet the empirical coefficient α, essential for numerical stability in free–surface flows, turns out to be too dissipative in practice, as mentioned by other authors [19], too. The present study focuses on wave heights, time– and ensemble–averaged velocity and free surface elevation distributions [18], as well as turbulent flow features, namely vorticity gradients and velocity spectra.

II. SPH MODEL – SPHYSICS

The SPH method's Lagrangian nature allows the unhindered simulation of free–surface flows with strong deformations, such as wave breaking (e.g. plunging) or wave–structure interaction in coastal areas, as described thoroughly in [20] and [21]. These and previous efforts have flourished and produced as a final outcome the SPHyics 'open source' model. Detailed presentation of the analytical features of the classical SPH formulations used in SPHysics can be found in the respective User Guide [14]. Only brief reference of the specific calibration features used is made here.

A. Basic SPHysics Features

The basic relation of the SPH approximation technique for an arbitrary property function, *A*, reads in discretized form:

$$A_i = \sum_j A_j \left(m_j / \rho_j \right) W_{ij} \qquad (1)$$

where *m*, ρ are the particle mass and density respectively, *i* and *j* the reference and surrounding compact support particles and W_{ij} a distance varied interpolation weighting function called 'kernel' and given analytically in various implemented versions [14], such as Gaussian, quadratic, cubic (B-spline), quintic (Wendland) etc. Probably the most important variable is the smoothing length *h*, which primarily controls the magnitude of the interpolation process throughout the domain and consequently the accuracy of computations. Moreover, instead of an additional arduous Poisson-type equation for the calculation of the pressure, the artificial compressibility approximation is included in the model, with the appointment of an equation of state [7]:

$$P = B\left[\left(\rho / \rho_o \right)^{\gamma} - 1 \right] \qquad (2)$$

where γ = 7, $B = c_0^2 \rho_0 / \gamma$, reference density $\rho_0 = 1000$ kgr/m^3, speed of sound $c_0 = \partial P / \partial \rho |_{\rho_0} = c_B \bullet V_{max}$, V_{max} the maximum velocity in the computations and c_B an artificial compressibility factor. By changing *B*, we can artificially modify the speed of sound to approach nearly incompressible conditions and speed up computations.

B. Special SPHysics Assumptions

Among its various assumptions, the code incorporates the classical, for the SPH literature, concept of an artificial empirical viscosity term Π*ij* in the NS equations:

$$\Pi_{ij} = -\alpha \mu_{ij} \bar{c}_{ij} / \bar{\rho}_{ij} \qquad (3)$$

where $\alpha \approx 0.01 \sim 0.1$, $\mu_{ij} = (u_i - u_j)\, r_{ij} / (r_{ij}2 + 0.01h^2)$, *u* = the velocity vector, *c* = the computational speed of sound and over–bared features denoting average property values between *i* and *j* particles. The empirical coefficient α is considered necessary for numerical stability, yet it may provoke excessive dissipative performance of the model [19]. Furthermore the eddy viscosity assumption (Boussinesq hypothesis) is also employed in the framework of a standard Smagorinsky–type model for the derivation of turbulent eddy viscosity as

$$\nu_t = [\min (C_s \, \Delta l)]^2 \, |S_{ij}| \qquad (4)$$

where Δl is inter–particle spacing, S_{ij} the strain rate tensor, and the Smagorinsky coefficient C_s equals 0.12. This approach gives rise to the ultimate Sub–Particle Scale (SPS) stress tensor symmetric formulation, which can be traced through equations (10) ~ (12) in [22]. Additionally, solid boundary conditions are dealt with as either dynamic or repulsive, based on the Lenard-Jones molecular potential [14]. The first approximation assumes boundary particles fixed in a staggered way, having the properties of the fluid particles, yet with zero velocities. The second one introduces repulsive forces between fixed, co–linear solid particles and fluid ones through the use of the Lennard–Jones molecular potential. Both treatments define a more or less slip boundary condition in the inviscid limits. Ultimately, the available numerical schemes comprise Predictor-Corrector (PC) and Verlet (V) type algorithms [14]. A choice of constant and small time step Δt ensures fulfilment of the Courant–Friedrichs–Lewy criterion, yet increases the computational time especially for fine resolution simulations.

III. EXPERIMENTAL DATA AND NUMERICAL SETUP

Various experimental setups implementing wave generation, propagation and near–shore wave breaking have been traced in the relevant recent literature, with one of them standing out [18]. The geometric and hydraulic features of the

experiment used as input data for the numerical wave tank simulations undertaken as validation of the SPHysics code are presented in Table I. Specifically the horizontal distances of the gauges from the wave–maker boundary position and further detailed description of the experimental setup can be found in [18] and [22].

TABLE I. WAVE FLUME CHARACTERISTIC FEATURES

Geometric and hydraulic features values			
Water Depth (m)	*Flume Horizontal Distance (m)*	*Flume Vertical Distance (m)*	*Bottom Slope*
0.34	11	0.6	0.05
Wave Height (m)	*Wave Period (sec)*	*Breaker Type*	
0.105	2.42	Spilling/Plunging	

A. Calibration Features

The various features calibrated have been incorporated in respective test series shown in Table II.

TABLE II. DESCRIPTION OF CALIBRATION FEATURES

Test Series	**SPHysics feature calibration description**
a	default SPHysics v.1.4 settings with SPS model
b	calibration of smoothing length *h*
c	change of kernel function
d	change of numerical scheme
e	calibration of artificial viscosity coefficient α
f	change of boundary conditions
g	calibration of coefficient *B* for pressure compressibility
h	reduction of horizontal distance L_x
i	use of laminar viscosity
j	change of both kernel & numerical scheme
k	change of time-step *dt*
l	calibration of both smoothing length *h* and coefficient *B*
m	calibration of smoothing length *h* and change of both kernel & numerical scheme
x	change of spatial discretization steps Δx and Δz

B. Values of Calibrated Parameters

The test cases employed, according to the distinctive calibrated parameters are presented in Table III. Test ‘a’ corresponds to the basic default calibration described in [22], from which we deviate by altering solitary or joint parameters. The basic, among them, appears to be the smoothing length $h = c_f (\Delta x^2 + \Delta z^2)^{1/2}$, where c_f is a calibration coefficient and Δx, Δz the horizontal and vertical initial spatial discretization respectively. Variation of its implementation and respective test numbers appear, as test series ‘b’ in Tables II and III (h = 0.92 ~ 2.02 m and Δx / h = 0.7686 ~ 0.3501). The types of kernel and numerical algorithm are also altered, in order to track their influence on the results and appear as test series ‘c’ and ‘d’ respectively. Further separate calibration through the viscosity treatment assumption is pursued, regarding SPS Smagorinsky type model in all cases, except ‘i’ (laminar viscosity) and test series ‘e’ (artificial viscosity), with the values of coefficient α presented in Table III. The artificial compressibility factor’s impact on simulations is examined by varying its value from 10 to 40 (test series ‘g’). Furthermore in test series ‘j’, ‘l’, and ‘m’ certain combinations of the above calibration endeavours are attempted. Simulations were also conducted with finer Δx, Δz = 0.01 m (test series ‘x’) and variable or smaller constant time step $\Delta t = 5 \cdot 10^{-5}$ sec (test series ‘k’). Finally the boundary conditions were considered repulsive with a staggered lattice type initial particle distribution, except for test case ‘f’, where dynamic solid boundaries were implemented.

TABLE III. TEST CASES BASED ON MAIN CALIBRATED PARAMETERS

Test Cases	**Calibrated Parameters**				
	c_f	*h (m)*	*Δx (m)*	*Δx/h*	*Kernel-Scheme*
a	0.92	0.0260	0.02	0.7686	Quadratic-PC
b	1.08	0.0305	0.02	0.6547	Quadratic-PC
b2	0.82	0.0232	0.02	0.8623	Quadratic-PC
b3	1.02	0.0288	0.02	0.6932	Quadratic-PC
b4	0.72	0.0204	0.02	0.9821	Quadratic-PC
b5	1.12	0.0317	0.02	0.6313	Quadratic-PC
b6	0.62	0.0175	0.02	1.1405	Quadratic-PC
b7	1.22	0.0345	0.02	0.5796	Quadratic-PC
b8	0.52	0.0147	0.02	1.3598	Quadratic-PC
b9	1.32	0.0373	0.02	0.5357	Quadratic-PC
b10	1.42	0.0402	0.02	0.4980	Quadratic-PC
b11	1.52	0.0430	0.02	0.4652	Quadratic-PC
b12	2.02	0.0571	0.02	0.3501	Quadratic-PC
Test Cases	*Viscosity*	**Test Cases**	c_B	**Test Cases**	*Kernel-Scheme*
e	α=0.05	g	30	c	Cubic-PC
e2	α=0.04	g2	40	c2	Gaussian-PC
e3	α=0.07	g3	20	c3	Wendland-PC
e4	α=0.03	g4	10	d	Quadratic-V
e5	α=0.08	**Test Case**	*Δx (m)*	**Test Case**	*Boundaries*
e6	α=0.02	x	0.01	f	Dynamic
e7	α=0.09	**Test Cases**	c_f	*h (m)*	*Kernel-Scheme*
e8	α=0.06	m1-3	1.12 ~ 1.32	0.6313 ~ 0.5357	Cubic-V
e9	α=0.01				
e10	α=0.10	m4-6	1.12 ~ 1.32	0.6313 ~ 0.5357	Wendland-V
i	laminar				

IV. RESULTS AND DISCUSSION

Characteristic preliminary results provided by [22] have shown either good qualitative or rather acceptable quantitative agreement between SPHysics simulations and experimental

data [18]. For example, the free surface elevation pattern is depicted by an apparent undular form, with wave breaking manifesting in an evident spilling form, which reshapes into a weak plunging one in the inner surf zone. An unaccounted for inconsistency at the coast boundary spotted in other authors' simulations [20] persists, probably due to excessive repulsive forces at the coastline marginal boundary. A streaming sequence of the instantaneous mappings of the output results reveals a weak plunging incident just as reported by [18], admitting plausible qualitative agreement. Preliminary simulation endeavours with finer spatial discretization somehow weaken the above discrepancies [22], [23].

A. Basic Comparison Results

In a recent study [19], comparative analysis between SPH simulations and experimental data results reveal good portrayal for regular and irregular wave propagation specifically for the areas near the wave–maker. The authors report that enfeeblement of performance of their model is observed at near–shore regions. Moreover, decrease of h and simultaneous increase of the dimensionless spacing factor $\Delta x/h$, combined with the use of the cubic (B-spline) kernel, provokes dramatic downgrading of their results compared with experimental data. In the present study the previous outcome is affirmed, also for the use of quadratic kernel. Continuing farther in the relevant analysis of the spacing factor's $\Delta x/h$ influence on SPHysics performance, an optimized value is provided, namely that of test case 'b7' (Table III). The latter is evidently illustrated in Fig. 1, where virtually coincidence of the results is shown, between experimentally and numerically derived wave heights, is strictly valid only for the pre–breaking and the inner surf–zone regions [22]. At intermediate gauges, in the vicinity of the experimentally traced breaking point, an excessively over–diffusive performance is still noticed, forcing the waves to an early spilling–type breaking situation. Reference [15] uses Riemann solvers and shows that this issue is somehow dealt with, thus revealing that classical SPH formulations used herein are characterized by inherent numerical drawbacks. Leaving that aside, the SPH–SPS model generally provides acceptable prediction of the wave height, only for the pre-breaking and inner surf-zone region, with an optimised case ('b7'). Further decrease of $\Delta x/h$ (cases b11, b12) does not address the issue, specifically in the wave breaking region, where simulations fail totally. This outcome was somehow expected, since exaggerated increase of h smoothes out excessively the shear and other important properties of the fluid flow. On the contrary, the mean surface elevation (wave setup) is very well predicted by the model, except for the marginal high and low values of h in our analysis (Fig.1, 3rd & 4th graphs). A supplementary annotation is that for higher h and consequently lower $\Delta x/h$ values, the visual output of the wave breaking eventually is modified from nearly spilling in test 'a' [22] to almost plunging, as suggested in [18]. Visual depiction of these results can be found in [23]. Moreover, the optimised choice of h induces better estimation for the magnitude of the maximum velocity at the propagating crest of the breaking wave. The roughly 1.5 times the theoretical value of celerity in shallow water, $c_t=(gd)^{1/2}$ is assessed as a better approximation compared to $0.8c_t$, derived formerly in test 'a' [22].

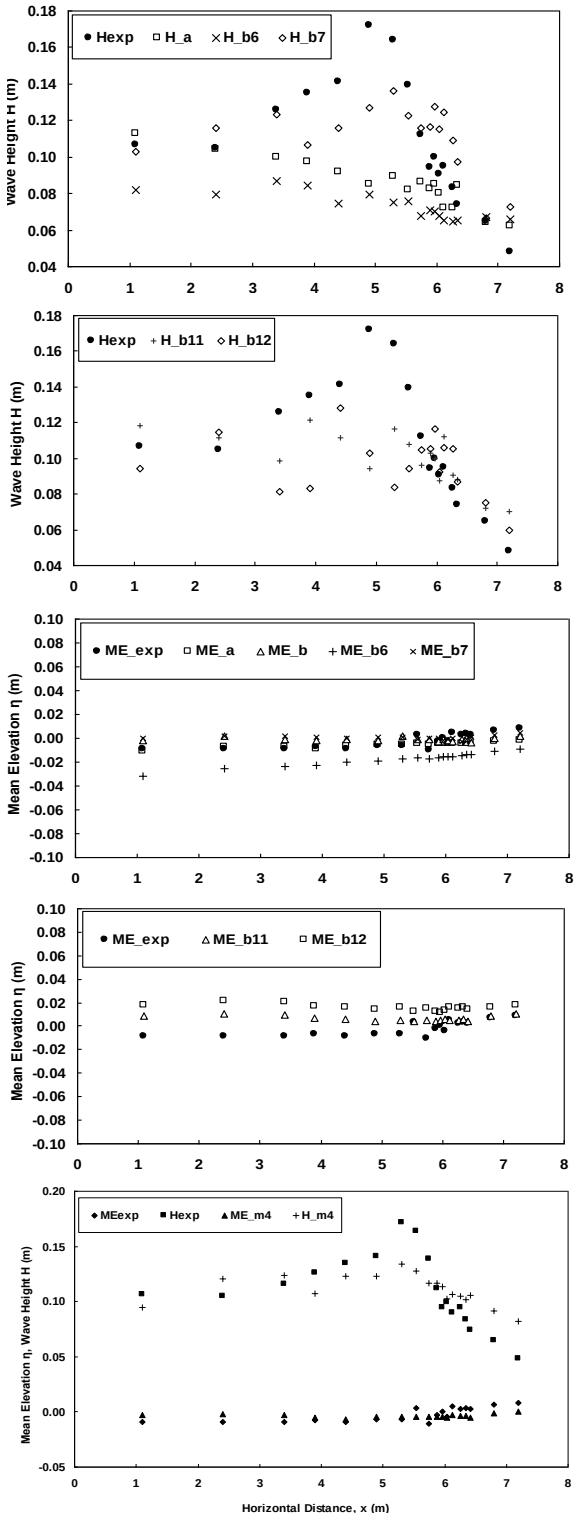

Figure 1. Comparisons of wave height 'H' and mean surface elevation 'ME' distributions between experiments [18] (exp) and characteristic simulations (test cases: a, b, b6, b7, b11, b12, m4)

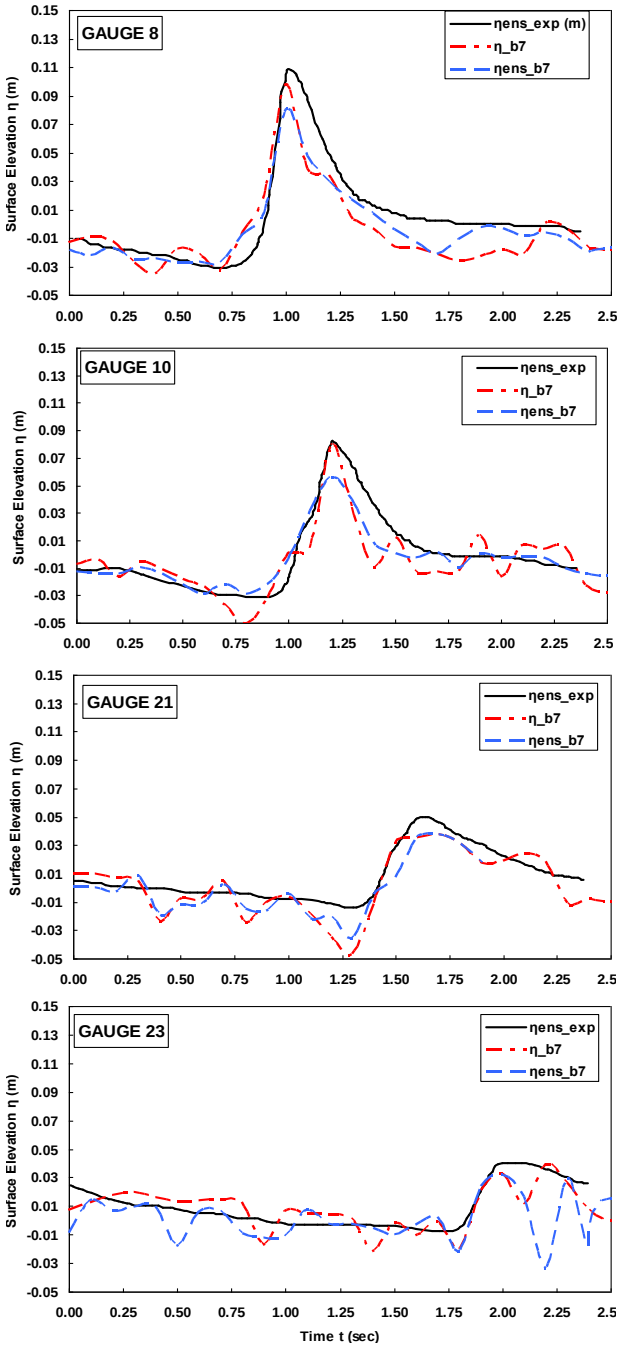

Figure 2. Comparison of ensemble–averaged free surface elevation in test case 'b7' (blue long dash) vs. experiments (black line) at gauges 8, 10 (incipient breaking region) and 21, 23 (inner surf zone).

Fig. 2 presents the ensemble–averaged [1] and real–time free surface elevation distributions (red short dash) of the SPHysics 'b7' simulations against experimental results [18]. The peak and trough drawdown is minimal compared to [22] results. In general there is an apparent small discrepancy in the incipient breaking region (gauges 8, 10), while in the inner surf zone (gauges 21, 23) the peak and trough drawdown cancel each other out revealing a good estimation of the wave height. Furthermore, calibration based on other parameters, such as c_B or the use of different kernels and numerical schemes, smaller time–steps etc, does not seem to attribute equally positive results compared to h and $\Delta x/h$ factors manipulation. The combined careful use of the above seems to be the advisable SPHysics calibration procedure, although this does not always provide the best results. For example in test case 'm', where the cubic kernel is used together with h emendation, we derive a much worse performance than case 'b7', especially in the inner surf zone. All in all it is expected, that through proper spatial discretization (Δx, Δz) calibration, we can observe higher quality representation of the plunging tongue detachment and impinging upon the forward trough as well as wave heights and free surface elevation reproduction. Besides, Fig. 3 portrays a similar as above sample of comparison for the depth– and ensemble–averaged velocities at the incipient breaking region for test 'a'. Resembling distribution patterns are detected throughout the whole computational domain with not such acceptable performance even during the implementation of the optimized calibration. This problematic behavior of the model relates directly to its inability to correctly reproduce the wave amplitudes at certain regions, yet probably also hinges on the fact that there are unsolved issues with computational viscosity and shear in the fluid. Additionally, as far as viscosity treatment is concerned, it has been argued in the past that the empirical coefficient α constitutes a numerical stability retainer, but becomes practically a factor of excessive dissipation in transient free surface flows [19]. Unlike the results of various other researchers, it seems really difficult hereby to adjust the model's calibration factor α, to cope with the data of [18], no matter what value is assumed inside the reasonable default limits of application (test series 'e'). Of course, no combined h and α calibration has been attempted in the present study, a probable eager cooperation to somehow bend the discrepancies. Preliminary results of vorticity gradient comparisons near the wave breaking region, like those shown below (Fig. 7), among the different implementations reveal absence of turbulent production in the incipient breaking region for the SPS model simulations and throughout the whole propagation domain for the artificial viscosity model ones. Visual verification of not plunging breaking supports the relevant argument also reencountered in a similar way in the test case 'a' simulation [22]. Thus, in order to replenish most of the previous presumptions, one can carefully consider Fig. 4, where comparisons of root mean square values of fluctuating free–surface elevation [18] and depth–averaged velocities are shown. The former is again approached somewhat better in test case 'b7' than other cases and the latter fails for all cases.

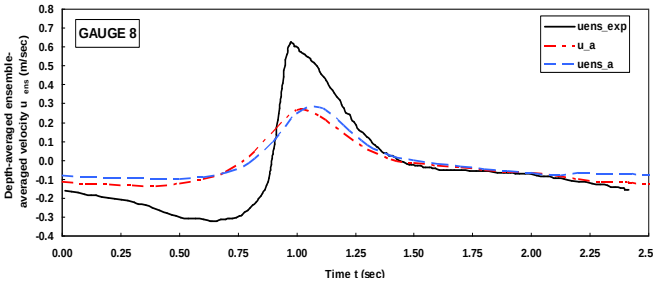

Figure 3. Comparison of ensemble–averaged velocities (blue long dash) and real–time velocities (red short dash) in test case 'a' vs. experiments (black line) at incipient breaking region

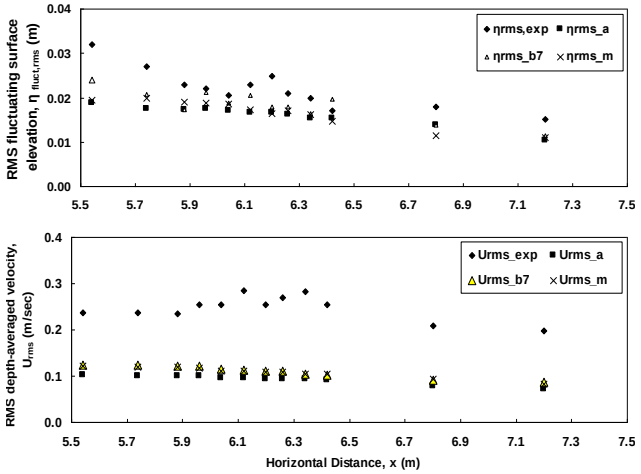

Figure 4. Comparison of variations of r.m.s. surface elevation fluctuation 'η' and depth–averaged velocity 'U' with distance from wave–maker, among experiments (exp) [18] and characteristic test cases (a, b7, m)

B. *Secondary Indicative Results*

Another interesting feature is presented in Fig. 5. The time–averaged, vertically distributed numerical values of the velocity vectors are shown at various gauges covering the whole of the surf zone, allowing us to clearly distinguish the undertow trend below the mean elevation from the near–surface net mass transport (Stokes's drift). The shear interface, in–between the two, is spotted at around the wave setup level, while the calculated trough envelope, based on wave amplitude, is located at z = 0.29 m. Characteristic values of depth–averaged undertow velocities and comparative presentation of the depth–averaged values of undertow and Stokes's drift is attempted through Fig. 6, between two characteristic test cases ('a' and 'b7'). In the questionable test case 'a' the mean seaward depth–averaged undertow is around 0.02 m/sec, whereas the mean shoreward depth–averaged Stokes's drift velocity is almost 0.43 m/sec. Its real value fluctuates from 0.27 m/sec, in the region near the breaking point, to 0.58 m/sec and 0.35 m/sec in the inner surf zone and the swash zone respectively. On the other hand in test case 'b7' corresponding values appear to be evidently higher (~0.023 and ~0.7 m/sec), yet at the same time the vertical distributions of time–averaged values follow exactly the same clearly plausible profile pattern. Adversely, the vertical profile pattern of vorticity differs substantially among the various test cases, consequently provoking diverse wave amplitude profiles.

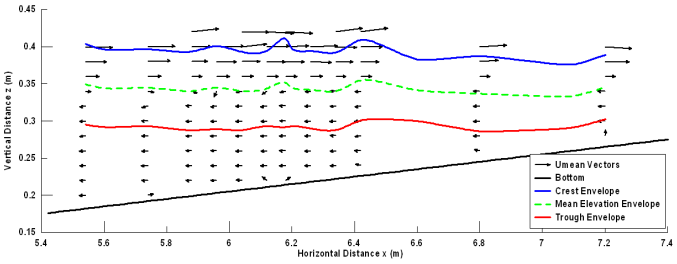

Figure 5. Time-averaged vertical distribution of velocity vectors at various gauges (8, 10-15, 17-19, 21, 23) covering the whole surf zone, clearly discriminating the undertow and Stokes's drift regions

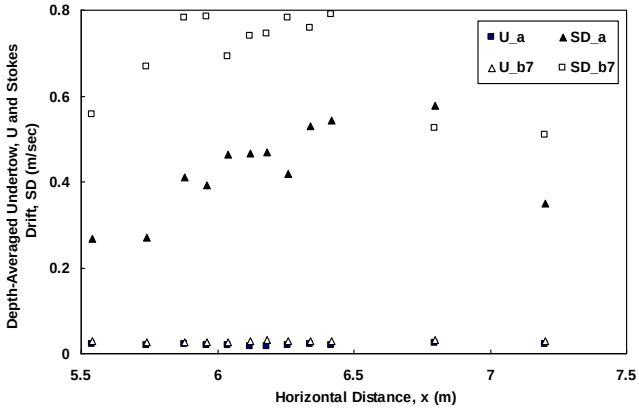

Figure 6. Comparison of depth–averaged undertow 'U' and Stokes's drift 'SD' distributions with horizontal distance 'x' for test cases a, b7

Thus, vertical profile distributions of the time-averaged horizontal velocities $\bar{u}$ and vorticity at characteristic gauges [18] are given in Fig. 7, where the vorticity ω can be derived from the following equation, written in discrete notation [24]:

$$\boldsymbol{\omega} = \vec{\nabla} \times \mathbf{u} = \sum_j m_j \left(\mathbf{u}_i - \mathbf{u}_j \right) \times \nabla_i W_{ij} \qquad (5)$$

Through careful inspection of the calculated vertical gradient evolution of vorticity with distance over the whole surf zone we can note that it exhibits lower values near the surface at gauges placed in the initial breaking region than the respective ones in the mid and inner surf zone. The relative graph is referred to test case 'b7'. The above comparison corroborates the outcome of the research composed in [22], since enfeeblement or even lack of plunging jet formation is indicated and consequent overturning and strong splash–up by an impinging jet on the forward trough is somewhat missed out by the model. The latter constitutes the primary mechanism of vorticity generation and augmentation due to turbulent production in wave breaking. The lack of it is still visually traceable in the incipient breaking region, yet the weak plunging event is more intense compared to the one in test case 'a' [22]. Please note that in both test cases the SPS turbulence closure model is employed. The use of alternative assumptions, such as plain laminar viscosity or artificial one, reveal totally different vorticity patterns, with smoothed out gradients, partly leading to absolute dissimilar type of wave breaking (just spilling) and final underestimation of the wave heights and other flow properties. Thus the SPS model is distinguished among the others, yet needs further calibration or enhancement. The most probable cause for the persisting discrepancies is the Smagorinsky–type model consideration of the respective C_s factor which is kept constant and equal to 0.12 throughout the whole computational domain, not taking into account the velocity vector field evolution and its spatial gradients. An ultimate important feature, with regard to turbulence in wave breaking, appears to be the spectral reproduction of the velocity field, through the Fast Fourier Transform of the fluctuating (turbulent) parts of the velocities, calculated by filtering the computationally derived velocity data.

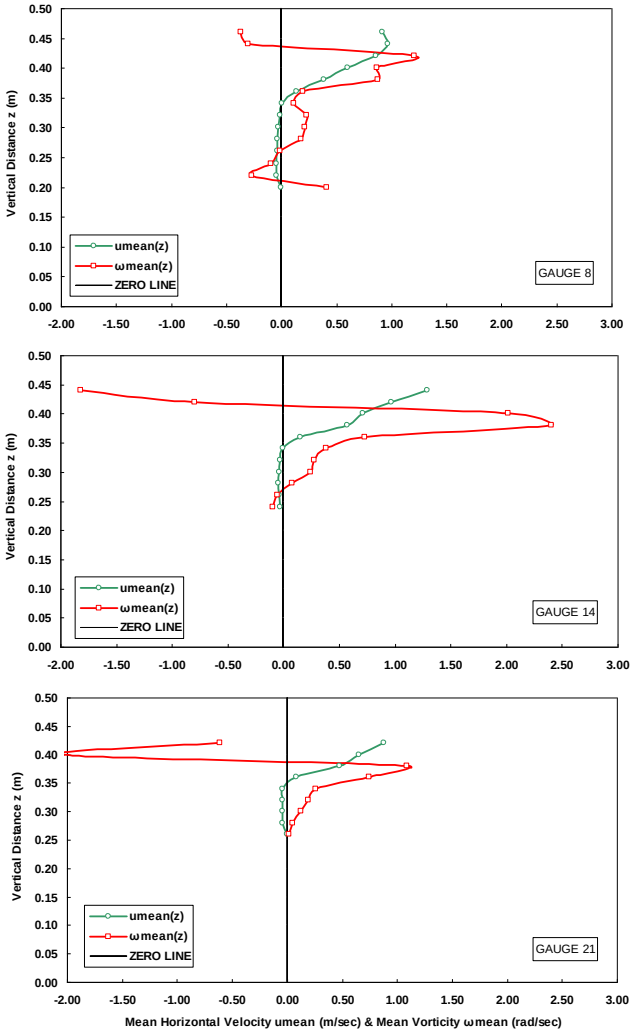

Figure 7. Test b7 time–averaged vorticity 'ω_{mean}' and horizontal velocity 'u_{mean}' vertical distributions at incipient, inner breaking and swash zones (gauges 8, 14, 21)

Following the work of [18] for experimental results, the horizontal and vertical velocity spectra, derived by the SPHysics produced velocity field, for test 'a' and initial breaking (gauge 8) at still surface level are presented in Fig. 8. Gradients of approximately −5/3 (on the log/log scale), typical of isotropic (inertial sub–range) turbulence, and −3, typical of two–dimensional frozen turbulence [25], are marked on the graphs, representing the gradient limits explored in [18]. The descending pattern of the computed velocity power spectrum follows approximately the gradient of −5/3 almost down to a frequency f of 10Hz. The background gradient close to −3 does not appear anywhere in the flow field in the present analysis. The above only occur at still water level throughout the entire surf zone region. At mid–depth no scaling law is apparent for any frequency band. The Nyquist filter frequency is about 25Hz and it is clear that random turbulence below this frequency is lost in the averaging process. The results kind of resemble, yet hardly agree with the experimentally derived ones [18], providing the analysis with the suspicion that the computationally derived turbulence is far from isotropic, especially for $f \geq 5$ Hz, where a horizontal trend of the power spectrum distribution manifests itself obviously, exceeding the respective marginal gradients.

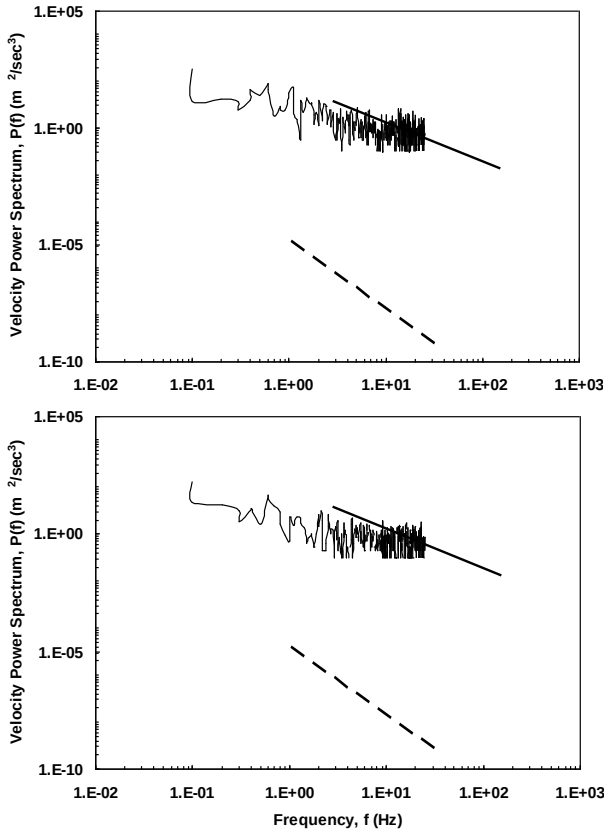

Figure 8. Horizontal (upper) and vertical (lower) velocity spectra for initial breaking (gauge 8), at still surface level. –5/3 (full line) and –3 (dashed line) log–log gradient are shown too. Ensemble averaging Nyquist filter is 25 Hz.

V. Conclusions and Suggestions

A. *Conclusions*

The newly edited 'open source' academic CFD code SPHysics [14] determining the computational framework for various implementations of the SPH method was validated against experimental data of wave propagation and breaking on smooth mild sloping beaches placed inside a laboratory scale wave flume [18]. Nearly all of the model's parameters were calibrated separately. Conclusively, plausible agreement is succeeded in terms of wave heights and bore front velocities, for one optimum dimensionless smoothing ratio. The combined use of the best numerical schemes, computational kernels and artificial compressibility manipulation seems promising and needs further attention, although preliminary relevant results do not excel that much. Among the various parameters involved the smoothing length is most important in shaping the results, followed as expected by the spatial resolution. Following previous efforts [19], [22] and [23] it can be said that, in general, prediction of wave heights is still acceptable only in the pre–breaking and inner surf zones, while the wave setup is finely estimated everywhere. The wave breaking process is somehow exaggerated in the incipient and mid–breaking region, with a consequent underestimation of wave

height there. Nonetheless promising results are provided in the framework of present proposals. The derived data comprise, among others, ensemble–averaged and r.m.s. free–surface elevation and velocities, with acceptable and short results respectively. Moreover, the undertow and Stokes's drift vertical and depth–averaged values are derived, establishing a clearly rational and stable qualitative pattern for all SPHysics calibrations. The same notion does not account for the vertical profiles of vorticity, among which differences are apparent and indicating that the turbulence models incorporated produce really diverse behaviour of the method. In particular the artificial viscosity concept does not succeed that well and presents an excessively over–diffusive behaviour. On the other hand the SPS Smagorinsky–type eddy viscosity model used for the closure of turbulence, in the type of LES-SGS models seems to treat the turbulent energy cascade from resolved to sub–particle scales rather poorly, especially in areas with great velocity gradients, although proves to be certainly more proficient than others. The probable reason for that infirmity is that the Smagorinsky coefficient is held constant all over the computational domain not taking into account the wider flow field evolution. In addition to that, turbulence back–scatter phenomena are also being neglected. Conclusively the computationally derived velocity spectra, using the SPHysics velocity field results, reveal a partly plausible trend compared to the experimental ones, yet even larger discrepancies, encountered in larger depth at nearly all of the gauges, mildly discredit the acute robustness of the SPS model.

B. Future SPHysics Perspectives

The spatial differentiation of the Smagorinsky coefficient, in reference to the various characteristic velocity field regions, such as wave propagation, breaking and swash zones and based upon comparisons with experiments, proves to be compulsory for SPH simulations and is proposed for prospective investigations. The latter seems to be a semi–empirical method with no guaranteed efficiency for all cases. Thus the use of a scientifically solid enhanced dynamic Smagorinsky–type model [26], based on Germano's identity [27] and taking into account, the spatial derivatives of the surrounding velocity field, is also proposed for future research. Further calibration of the SPHysics model in terms of turbulent features requires of course the implementation of three–dimensional simulations, which are expected to yield even better results. Further analysis and determination of the turbulent kinetic energy and its dissipation rate in the various scales should enlighten this issue.

ACKNOWLEDGEMENT

C. V. M. would like to thank Dr B. Rogers and Prof. P. Stansby for their advice and comments.

REFERENCES

[1] K. Nadaoka, M. Hino and Y. Koyano, "Structure of the turbulent flow field under breaking waves in the surf zone", in J. Fluid Mech., 1989, vol. 204, pp. 359–387.

[2] J. Grue, P. L. F. Liu and G. K. Pedersen (Eds), "PIV and water waves", Advances in Coastal & Ocean Engineering, vol. 9, World Scientific Publishing, 2003.

[3] S. Longo, M. Petti and I. J. Losada, "Turbulence in swash and surf zones: a review", in Coastal Engineering, 2002, vol. 45, pp. 129–147.

[4] E. D. Christensen, "Large eddy simulation of spilling and plunging breakers", in Coastal Engineering, 2006, vol. 53, pp. 463–485.

[5] B. Elfrink and T. Baldock, "Hydrodynamics and sediment transport in the swash zone: a review of perspectives", in Coastal Engineering, 2002. vol. 45, pp. 149–167.

[6] J. J. Monaghan, "Smoothed particle hydrodynamics", in Ann. Rev. Astron. Appl., 1992, vol. 30, pp. 543–574.

[7] J. J. Monaghan, "Smoothed particle hydrodynamics", in Rep. Prog. Phys., 2005, vol. 68, pp. 1703–1759.

[8] M. Gómez-Gesteira, B. D. Rogers, R. A. Dalrymple and A. J. C. Crespo, "State–of–the–art of classical SPH for free–surface flows", in J. of Hydraulic Research, 2010, vol.48 (Extra Issue), pp. 6–27.

[9] J. J. Monaghan, "On the problem of penetration in particle methods", in J. Comput. Phys., 1989, vol. 82, pp. 1–15.

[10] A. Colagrossi and M. Landrini, "Numerical simulation of interfacial flows by smoothed particle hydrodynamics", in J. Comput. Phys., 2003, vol. 191, pp. 448–75.

[11] G. A. Dilts, "Moving least squares hydrodynamics: consistency and stability", in Int. J. Numer. Methods, 1999, vol. 44, pp. 1115–55.

[12] J. Bonet and T. S.–L. Lok, "Variational and momentum preservation aspects of smooth particle hydrodynamic formulations", in Comput. Methods Appl. Mech. Eng., 1999, vol. 180, pp. 97–115.

[13] J. J. Monaghan, "SPH without a tensile instability", in J. Comput. Phys., 2000, vol. 159, pp. 290–311.

[14] M. Gómez–Gesteira, B. D. Rogers, R. A. Dalrymple, A. J. C. Crespo and M. Narayanaswamy, "User guide for the SPHysics code, v1.4", 2008, http://wiki.manchester.ac.uk/sphysics.

[15] B. D. Rogers, R. A. Dalrymple and P. K. Stansby, "Simulation of caisson breakwater movement using SPH", in J. of Hydraulic Research, 2010, vol. 48, pp. 135–141.

[16] R. Xu, P. Stansby and D. Laurence, "Accuracy and stability in incompressible SPH (ISPH) based on the projection method and a new approach", in J. of Computational Physics, 2010.

[17] D. Violeau, "Application of SPH to industrial cases and turbulence modelling", presentation in SPH Lectures Series, Univ. of Manchester, 8-9 April 2010.

[18] P. K. Stansby and T. Feng, "Kinematics and depth–integrated terms in surf zone waves from laboratory measurement", in J. Fluid Mech., 2005, vol. 529, pp. 279-310.

[19] D. De Padova, R. A. Dalrymple, M. Mossa and A. F. Petrillo, "SPH simulations of regular and irregular waves and their comparison with experimental data", 2009, arXiv, arXiv:0911.1872v1.

[20] R. A. Dalrymple and B. D. Rogers, "Numerical modeling of water waves with the SPH method", in Coastal Engineering, 2006, vol. 53, pp. 141–147.

[21] A. J. C. Crespo, M. Gómez–Gesteira and R. A. Dalrymple, "3D SPH simulation of large waves mitigation with a dike", in J. Hydr. Res., 2007, vol. 45, pp. 631–642.

[22] C. V. Makris, C. D. Memos and Y. N. Krestenitis, "Numerical simulation of near–shore wave breaking using SPH method', Proc. 4th SCACR, Barcelona, Spain, 15–17 June 2009.

[23] C. V. Makris, C. D. Memos and Y. N. Krestenitis, "SPH numerical simulation of surf zone characteristics", Proc. 6th ISEH, IAHR, NTUA, TEE, Athens, Greece, 23-25 June 2010, (in press).

[24] A. J. C. Crespo, M. Gómez–Gesteira and R. A. Dalrymple, "Vorticity generated by a dam break over a wet bed modeled by smoothed particle hydrodynamics", Proc. 32nd IAHR Congress, CORILA, 2007.

[25] M. Lesieur, "Turbulence in fluids', 2nd edition Kluwer, 1990.

[26] D. K. Lilly, "A proposed modification of the Germano subgrid–scale closure method", in Phys. Fluids A, 1992, vol. 4(3), pp. 633-635.

[27] M. Germano, U. Piomelli, P. Moin and W. H. Cabot, "A dynamic subgrid–scale eddy viscosity model", in Phys. Fluids A, 1991, vol. 3(7), pp. 1760-1765.